N. Schmitz, C. Schwotzer, H. Pfeifer, J. Schneider, E. Cresci, J. G. Wünning

Development of an Energy-Efficient Burner for Heat Treatment Furnaces with a Reducing Gas Atmosphere*

Entwicklung eines energieeffizienten Brenners für Wärmebehandlungsanlagen mit oxidationsträger/reduzierender Schutzgasatmosphäre

Abstract/Kurzfassung

One of the main reasons for metal loss of semi-finished metal products during heating in reheating and heat treatment furnaces is scale formation. In the presented project a burner is developed which produces a low oxidizing / reducing atmosphere in the furnace. The concept is realized by a recuperative burner, which generates a reducing furnace atmosphere due to fuel rich combustion of natural gas and air. The complete combustion of the furnace atmosphere is ensured by the injection of additional air and takes places in an open radiant tube resulting in a high energy efficiency. In this paper numerical and experimental results are presented and discussed. The numerical results showed the huge impact of the secondary air swirl on the post-combustion in the annular gap which is formed between the open radiant tube and the burner. Mixing phenomena in the annular gap results in a nearly complete post-combustion at low and high swirl angles of the additional combustion air ($\omega = 0^{\circ}$, $\omega = 90^{\circ}$). Instead of that, at a swirl angle of $\omega = 45^{\circ}$ the entire reaction from CO to CO₂ was not ensured within the boundaries of the numerical model. The quality of the post-combustion was experimentally evaluated by measuring the CO-emissions in the off-gas channel. These were lower than 50 mg/m³ in a wide range of operation. The NO_x -emissions are lower than 121 mg/m³ at all tested cases.

Keywords: Scale-free reheating, post-combustion, recuperative burner, direct fired furnace, fuel rich combustion

Einer der Hauptgründe für Metallverluste im Bereich der Erwärmung von Metall-Halbzeugen ist die Zunderbildung in Erwärmungs- und Wärmebehandlungsöfen. Das vorgestellte Projekt behandelt die Entwicklung eines Brenners, mit dem sich eine schwach oxidierende bzw. reduzierende Ofenatmosphäre einstellen lässt. Realisiert wird das Konzept durch gasbeheizte Rekuperatorbrenner, die durch die unterstöchiometrische Verbrennung von Erdgas und Luft eine reduzierende Atmosphäre direkt im Ofen erzeugen. Der vollständige Ausbrand der noch brennbaren Ofenatmosphäre erfolgt mit zusätzlicher Verbrennungsluft in einem offenen Strahlheizrohr, wodurch hohe Wirkungsgrade erzielt werden. Die numerischen Voruntersuchungen beschreiben den Einfluss des Eintrittswinkels der Sekundärluft auf die Nachverbrennung der Ofenatmosphäre im Ringspalt, der sich zwischen dem Strahlrohr und dem Brenner befindet. Mischungsphänomene im Ringspalt verursachen eine nahezu vollständige Nachverbrennung bei kleinen und großen Drallwinkeln ($\omega = 0^{\circ}$, $\omega = 90^{\circ}$). Bei einem Drallwinkel von ($\omega = 45^{\circ}$) kann der vollständige CO-Ausbrand in den Grenzen des numerischen Modells nicht sichergestellt werden. Die Abgasemissionen wurden durch Messungen im Abgaskanal experimentell untersucht. Die CO-Emissionen liegen für einen weiten Bereich unter 50 mg/m³. Die NO_x-Emissionen betragen für alle untersuchten Parameterkonstellationen weniger als 121 mg/m³. ■

Schlüsselwörter: Zunderarme Wiedererwärmung, Nachverbrennung, Rekuperatorbrenner, direkte Beheizung, unterstöchiometrische Verbrennung

Authors/Autoren: Nico Schmitz, M. Sc., RWTH Aachen University – Department for Industrial Furnaces and Heat Engineering (IOB), Kopernikusstr. 10, 52074 Aachen, Deutschland, schmitz@iob.rwth-aachen.de (Corresponding author/Kontakt)

Christian Schwotzer, M. Sc., Univ.-Prof. Dr.-Ing. Herbert Pfeifer, RWTH Aachen University – Department for Industrial Furnaces and Heat Engineering (IOB)

Julia Schneider, B. Eng., Enrico Cresci, M. Sc., Dr.-Ing. Joachim G. Wünning, WS Wärmeprozesstechnik GmbH, Dornierstr. 14, 71272 Renningen, Deutschland

1 Introduction

One application for direct fired reheating furnaces is the heating of slabs or billets prior to the hot forming process. To ensure a high thermal efficiency, these furnaces are usually direct fired with natural gas and air. A complete combustion and high energy efficiency is realized by an operation with excess air [1]. Besides temperature, time and the chemical composition of the workpiece, the furnace atmosphere has an important influence on the formation of scale [2, 3]. Within the furnace atmosphere, free oxygen, carbon

dioxide and vapor cause an oxidation of the surface of the product [4, 5]. Prior to the hot working, the scale has to be removed from the surface, resulting in a metal loss of up to 5 % [6].

Protective gas furnaces avoid scale formation. These furnaces are usually electrically heated or heated by gas fired radiant tubes. Typically forming gas, exothermic or endothermic gases produced by incomplete combustion of hydrocarbons, are used in these furnaces [7]. *Schmidt* et al. and *Schwotzer* et al. present a method to decrease the formation of scale by fuel rich combustion [6, 8-10]. Fuel rich combustion of natural gas and air (λ < 1) delivers atmospheres containing carbon monoxide (CO), carbon dioxide (CO₂), hydrogen (H₂), vapor (H₂O_(g)) and nitrogen (N₂) [11]. In this paper the air ratio λ is defined as the reciprocal value of the equivalence ratio φ , defined in Equation (1), whereas λ < 1 is defined as fuel rich and λ > 1 is defined as fuel lean.

$$\lambda = \frac{1}{\phi} \tag{1}$$

The results of *Schmidt* et al. [6] show the possibility to decrease the metal loss in steel reheating up to 33 % by using fuel rich combustion with an air ratio of $\lambda = 0.95$. *Schwotzer* et al. [10] determined that copper can be reheated without forming an oxide scale on the surface in an atmosphere with an air ratio of $\lambda = 0.96$.

The presence of CO as a toxic gas requires a post-combustion. It is also necessary to ensure the complete usage of the fuel energy content for the reheating process.

In this project a burner was developed producing a low oxidizing/reducing atmosphere in the furnace with a thermal efficiency comparable to modern recuperative burners. This was realized by the combination of direct, fuel rich firing and indirect heating with open radiant tubes. The concept is shown in Figure 1.

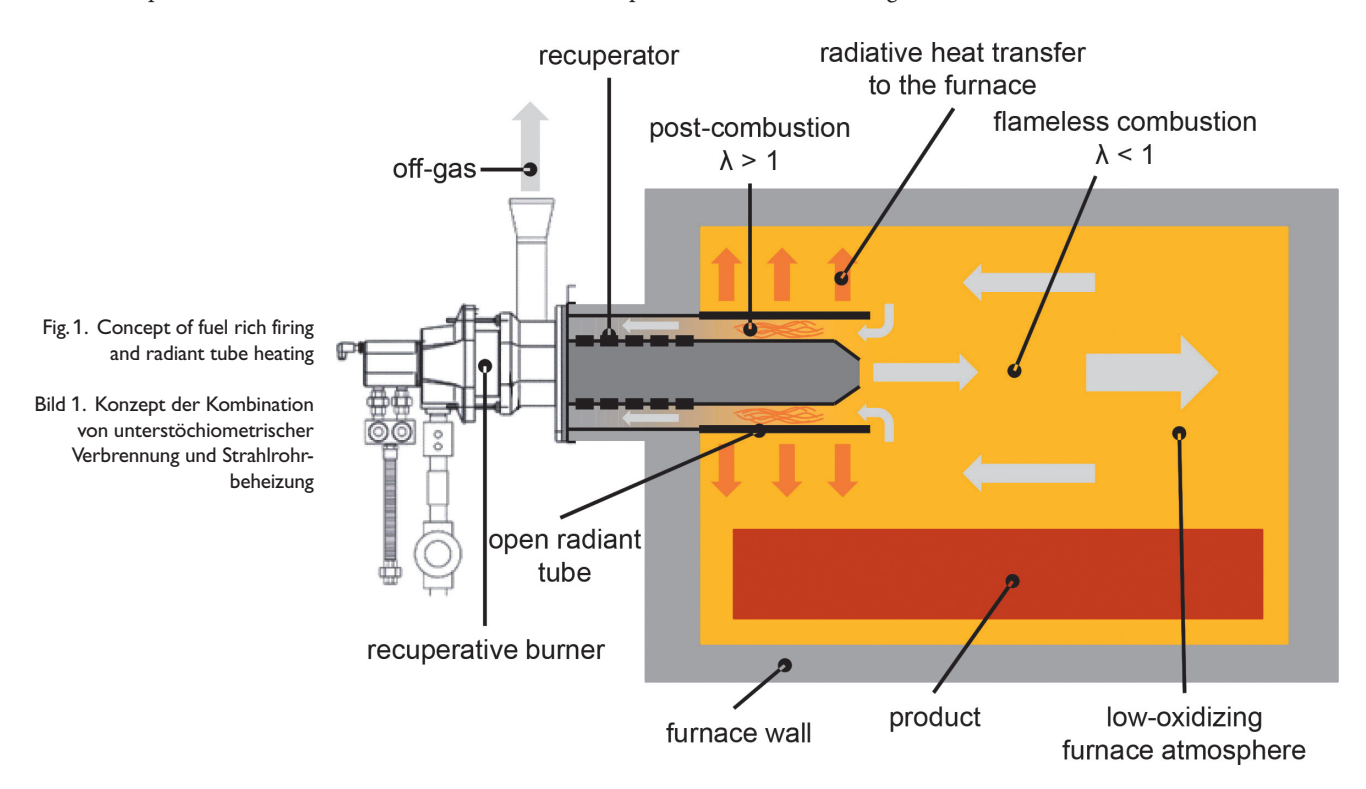
The primary combustion is fuel rich (λ < 1) and flameless (FLOX*) to realize a low oxidizing/reducing atmosphere and a uniform temperature distribution in the furnace. A concept-

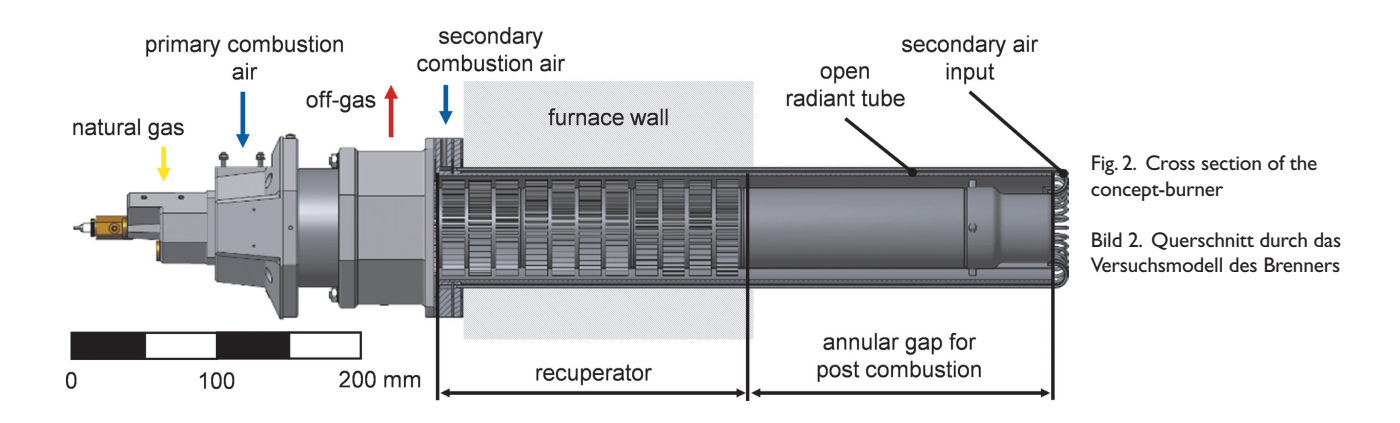
burner and an experimental setup were built up. The conceptburner has an open radiant tube (ORT) which creates an annular gap between the burner and the tube. In this annular gap, the post-combustion of the unburned species in the off-gas takes place by the addition of secondary air. The heat of the combustion is recuperated to heat up the primary and secondary combustion air and transferred to the furnace by radiation of the ORT. The concept-burner was used to determine experimental operating conditions for the further development of a ceramic, high temperature prototype.

Via CFD methods the post-combustion was investigated numerically to quantify the influence of different parameters like the width of the annular gap and the swirl angle of the secondary combustion air. The numerical model was validated by temperature and gas composition measurement in the annular gap of the concept-burner at an experimental setup. Additionally, the operation limits, the performance of heat recovery and the CO- and $\rm NO_{X^-}$ emissions were studied experimentally. The concept-burner was made of metallic components and the maximum operation temperature is limited to 1050 °C. The prototype is ceramic and operates at temperatures up to 1250 °C and therefore can also be used in applications like the reheating of steel in forging furnaces.

2 Experimental setup

The experimental setup consists of a concept-burner and a combustion chamber. The concept-burner is an extended recuperative burner equipped with an open radiant tube (ORT), forming an annular gap with a width of 15 mm between the burner and the ORT. Figure 2 shows the cross section of the modified burner. A picture of the operating burner in a furnace is shown in Figure 3. The outer diameter of the ORT is 145 mm and the free length of the ORT in the furnace is 425 mm. The recuperator is placed in the furnace wall. Its length is 400 mm.





For a high thermal efficiency, the air used for primary combustion is preheated in the recuperator. The combustion efficiency η_c is defined according to [1] in Equation (2).

$$\boldsymbol{\eta}_{c} = 1 - \frac{\dot{H}_{off-gas}}{\dot{H}_{fuel}} = 1 - \frac{\dot{m}_{off-gas} \cdot c_{p,avg,off-gas} \cdot (T_{off-gas} - T_{ambient})}{\dot{V}_{fuel} \cdot H_{i,fuel}} \tag{2}$$

The fuel enthalpy \dot{H}_{fuel} was estimated by multiplying the standard volume flow \dot{V}_{fuel} with the net calorific value $H_{i,fuel}$. The off-gas enthalpy $\dot{H}_{off\text{-}gas}$ was calculated by the off-gas mass flow $\dot{m}_{off\text{-}gas}$, the averaged specific heat capacity $c_{p,avg,off\text{-}gas}$ and the temperature difference between the off-gas temperature $T_{off\text{-}gas}$ and the ambient temperature $T_{ambient}$. As a result, lower off-gas temperatures result in a higher combustion efficiency and therefore in a higher thermal efficiency of the furnace.

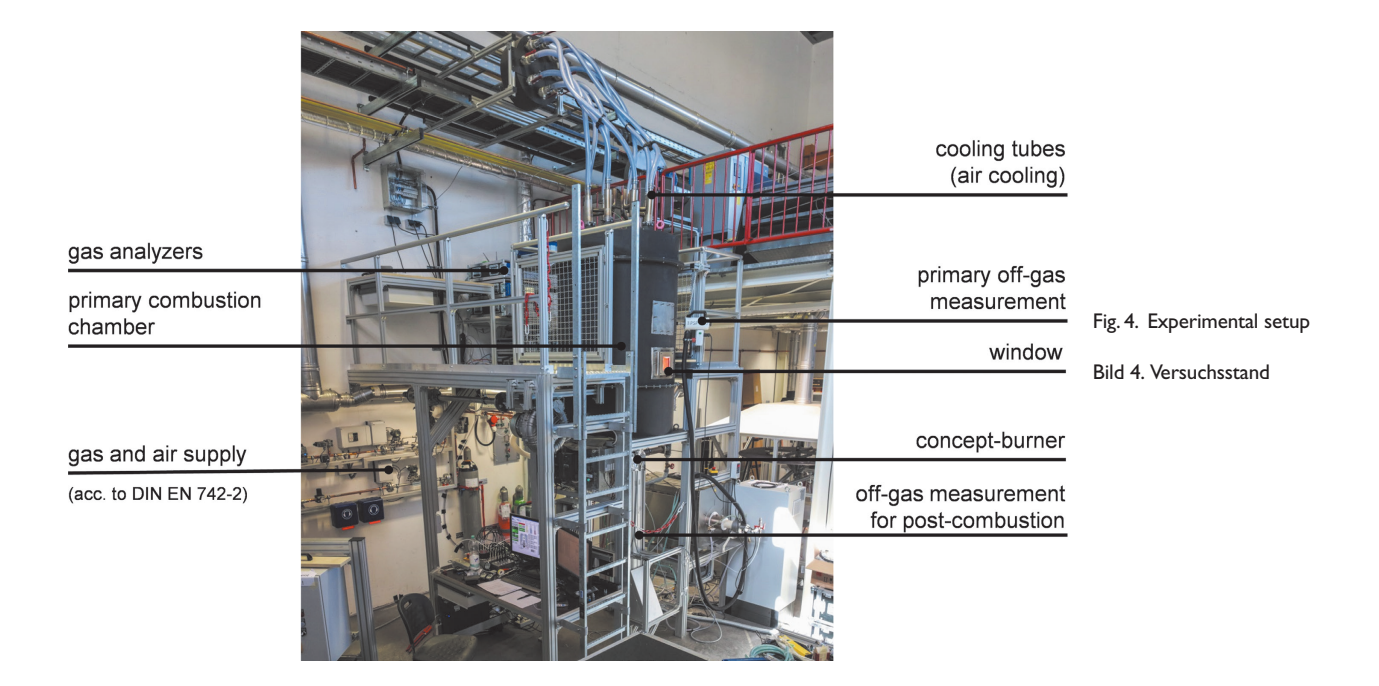
The primary off-gas contains unburnt species like CO and $\rm H_2$. These species are post-combusted in the annular gap by the addition of secondary air. The additional combustion air is directed in the annular gap at a defined angle, causing a turbulent swirl in the gap which strongly affects the quality of the post-combustion. The burned off-gas leaves the furnace throughout the recuperator and the off-gas channel.

The sensible enthalpy of the fully combusted off-gas is transferred to the furnace by convection and radiation over the surface



Fig. 3. Concept-burner operating at the experimental setup

Bild 3. Versuchsmodell des Brenners im Betrieb



of the ORT or to the primary combustion air in the recuperator. Thus, the heat of the post-combustion is partially used directly in the furnace before the off-gas passes the recuperator. This results in a decrease in off-gas temperature before the recuperator and consequently, a combustion efficiency that is comparable to state-of-the-art recuperative burners.

The experimental setup is shown in Figure 4. The height of the primary combustion chamber is 950 mm and the inner diameter is 600 mm. The combustion chamber is equipped with an indirect air cooling system. The inner wall temperature of the furnace is measured at several positions, using type K thermocouples. The concept-burner is installed at the bottom of the chamber and supplied with natural gas (acc. to DIN EN 746-2) and air. Due to several modifications an off-gas sample probe and a suction pyrometer are installed to measure the off-gas composition and temperature in the reaction zone of the annular gap.

To control the furnace atmosphere, the mass flow of natural gas and primary combustion air are measured and controlled continuously. In addition, the primary off-gas composition is measured in the combustion chamber. Samples are taken with a heated sample probe and continuously transported to the gas analyzer after gas conditioning. The species CO, CO_2 , CH_4 , H_2 and O_2 are detected in the dry off-gas by infrared and paramagnetic analyzers.

To control temperature and emissions of the post-combustion the off-gas temperature and the gas-composition are measured additionally behind the recuperator. Thereby CO, NO and NO_2 , but also O_2 and CO_2 are detected.

3 Numerical calculations of post-combustion

For the CFD-calculations the commercial solver ANSYS* Fluent 16.2 was used. Due to the axial symmetry of the burner only 1/16

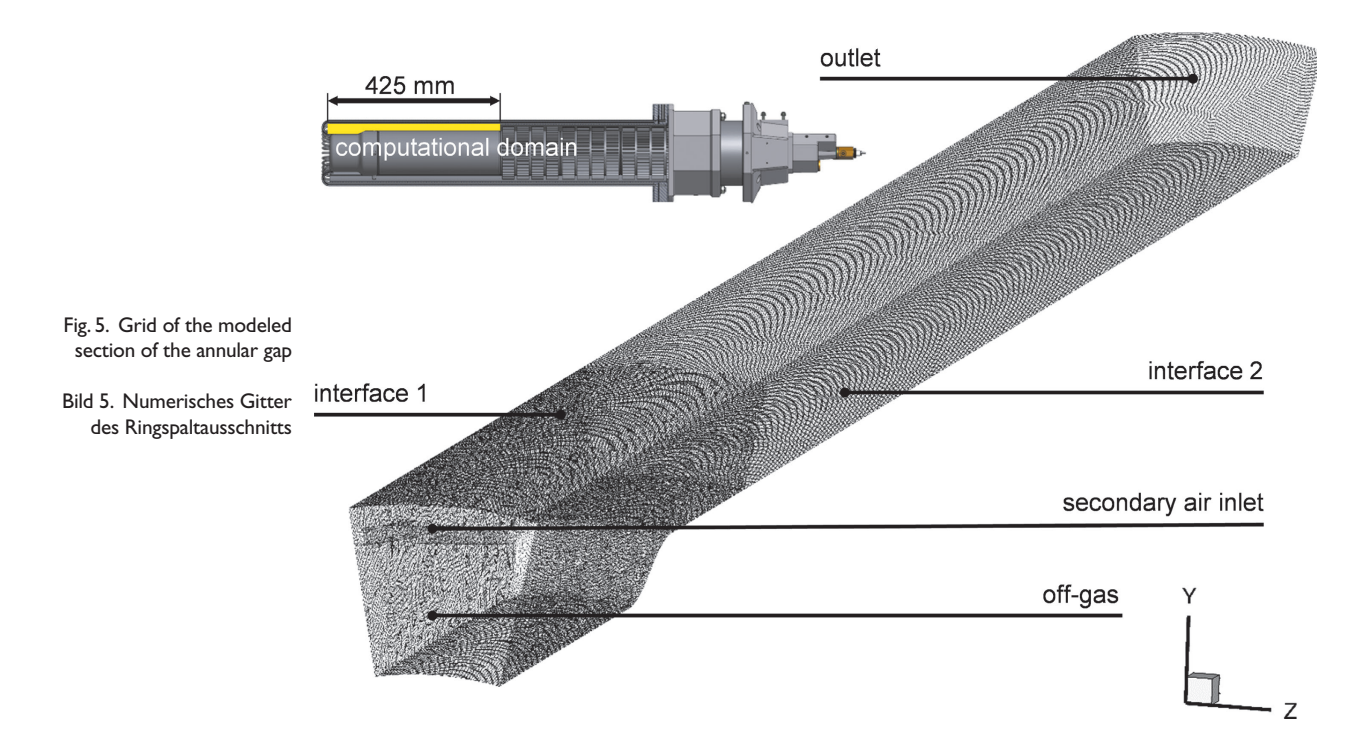
of the annual gap between the ORT and the burner were modeled. The modeled area is shown in Figure 5. The computational domain was reduced to the gas volume between the primary off-gas inlet and the recuperator inlet, which is also the outlet of the ORT, because this is the part of the burner where the combustion takes place. To describe swirl effects, a periodic boundary condition was used at the interfaces 1 and 2. All calculations were done at a steady state because the time averaged performance of the post-combustion system was described. Prior to the final calculations, a grid study delivered an unstructured grid composed of about 2.6 million hexahedral and tetrahedral cells.

A Shear-Stress-Transport-Model (koo-SST) by *Menter* [12] was chosen for turbulence modeling. As not only the fluid flow but also the combustion and heat transfer is described by the model, the chemical reactions were calculated with the eddy-dissipation-concept model by *Magnussen* with the DRM19 reaction set¹ [13]. Due to the high temperatures radiation has to be taken into account. Therefore, the Discrete Ordinates Model was chosen and absorption coefficients of the off-gas were calculated by the weighted-sum-of-grey-gases model.

4 Results

4.1 Impact of swirl on the post-combustion

A numerical investigation on the impact of swirl on the post-combustion was carried out prior to the manufacturing of the concept-burner. Methane with a constant volume flow of 4.01 m³/h was used as fuel in the CFD calculations, leading to a burner capacity of 40 kW. The primary air ratio was $\lambda_{\rm primary} = 0.80$, the total air ratio was $\lambda_{\rm total} = 1.05$. The input of secondary air was realized with small tubes as inlets, causing the formation of a free turbulent jet



¹ Kazakov, A.; Fenklach, M.: DRM 19 -Mechanism, URL: http://www.me.berkeley.edu/drm/

primary off-gas		secondary air		composition in vol%				
mass flow in kg/s	temperature in °C	mass flow in kg/s	temperature in °C	СО	CO ₂	H ₂	H ₂ O	N ₂
7.36098e-04	1100	2.144140e-04	800	4.0	7.0	4.8	17.3	bal.

Table 1. Boundary conditions for the numerical simulations

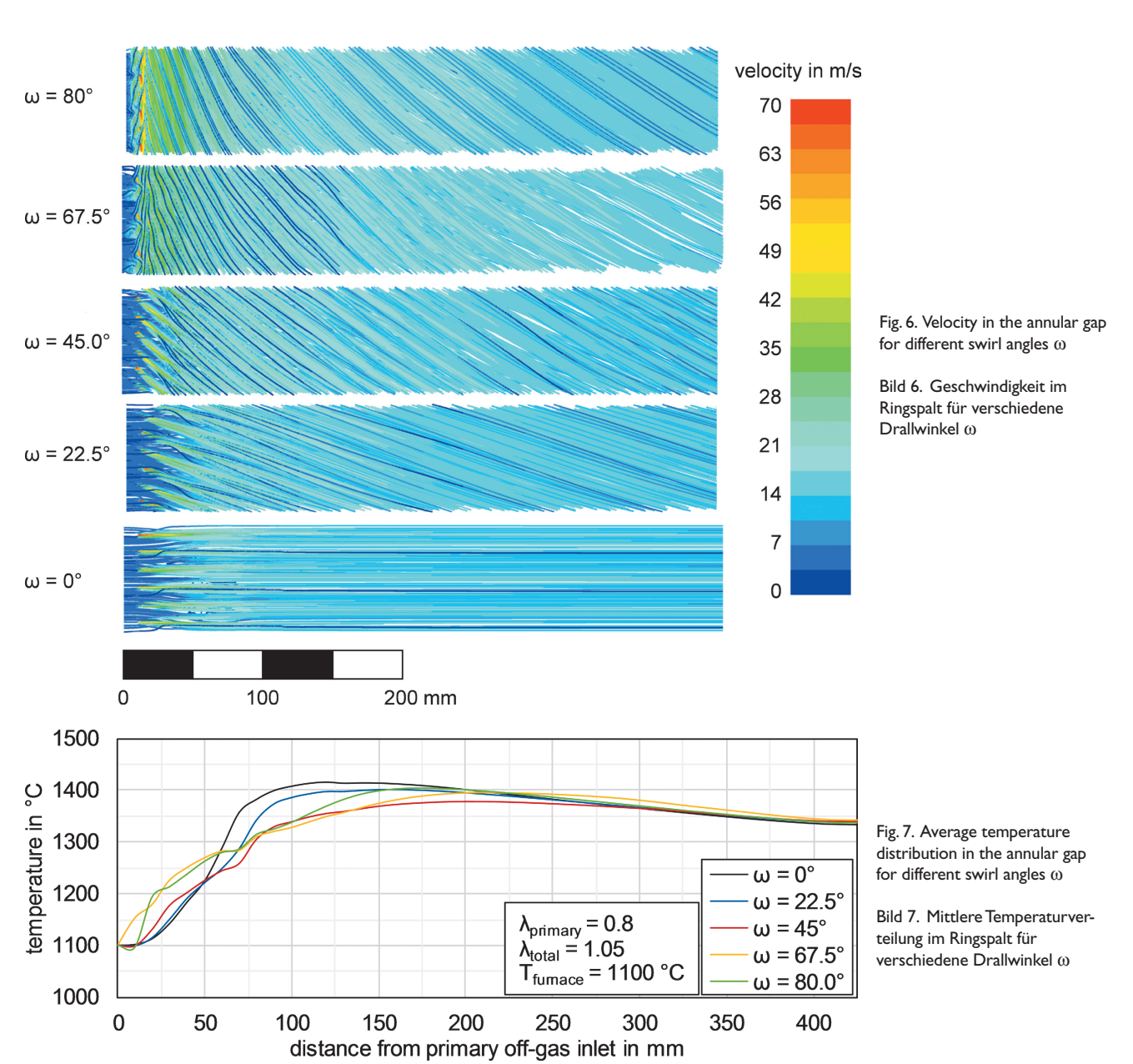
Tabelle 1. Randbedingungen der numerischen Simulation

to ensure intensive mixing. The furnace temperature was constant 1100 °C. Table 1 shows the primary off-gas composition, mass flows and temperatures which describe the boundary conditions for all cases.

The influence of a variation of the swirl angle ω on the velocity in the annular gap is shown in Figure 6. The streamlines are colored by the velocity magnitude for five different swirl angles. The secondary air inlet is positioned slightly behind the off-gas inlet. The off-gas entering the computational domain has an average ve-

locity of 5.8 m/s, the secondary air enters the model at the inlets with a velocity 70 m/s. Because of the high momentum of the secondary air, the flow in the annular gap is strongly affected by the inlet angle and there is an increase of the average velocity with an increasing swirl angle.

The results for the average temperature distribution in the annular gap are shown in Figure 7. The inlet temperature is a constant boundary condition and therefore similar for each case. The outlet temperatures are in a range between 1333 °C and 1343 °C.



Without any swirl ($\omega=0^\circ$) there is a sharp increase in temperature in the annular gap up to a position of about 75 mm, where the annular gap gets narrow by construction, see Figure 2. The maximum temperature of 1414 °C is reached at about 120 mm from the primary off-gas inlet. Higher swirl angles lead to a backward shift of the position of the maximum temperature. The lowest maximum temperature is reached at a swirl angle of $\omega=45^\circ$.

Another focus of interest was the post-combustion of the offgas, especially the CO emission, because the emissions are strongly regulated by law, i. e. in [14]. The CO concentration along the annular gap for different swirl angels is shown in Figure 8. Without swirl, a fast post-combustion reaction is realized, resulting in a CO concentration of 200 ppm at the outlet of the annular gap. A high swirl angle of $\omega=80^\circ$ also causes a fast reaction of carbon monoxide and a CO concentration of only 109 ppm at the outlet. At a swirl angle of $\omega=45^\circ$ the CO concentration at the end of the annular gap has the highest value with a concentration of about 700 ppm.

For a better understanding of the post-combustion phenomena in the annular gap the distribution of the CO concentration in the cross sections of the annular gap were plotted at the different swirl angles. The corresponding contour plots are shown in Figure 9. At the primary off-gas inlet the CO concentration is 4.0 vol.-%. Due to the addition of secondary air the post-combustion started.

At a swirl angle of $\omega > 0^\circ$, the swirl leads to a drift of the secondary air to the outer boundary of the annular gap towards the ORT. Therefore, there is a separation between air and off-gas, especially at

a swirl angle of $\omega=45^\circ$ and the mixing is less intensive compared to a swirl angle of $\omega=0^\circ$. This results in a high CO concentration at the outlet of the annular gap. With an increasing swirl angle of $\omega>45^\circ$, the radial velocity of the secondary air flow increases, resulting in an even stronger separation between off-gas and air. In combination with the reduction of the cross section of the annular gap, there is more turbulence at the beginning of the annular gap and therefore a better mixing of off-gas and air. Figure 10 shows the CO concentration at the outlet of the annular gap for different swirl angles.

The differences in the mixing performance correspond to the temperature distribution and the profiles of the CO concentration. With a swirl angle of more than 45° the velocities increase, causing an increase in turbulence and a better mixing performance. This has a positive effect on the post-combustion.

4.2 Experimental measured off-gas emissions

In the first experimental trials a swirl angle of $\omega=45^{\circ}$ was chosen. All cases were carried out at a nominal volume flow of natural gas of 4.00 m³/h according to the numerical investigations and the nominal burner capacity after post-combustion was 40 kW.

For different primary air ratios, the primary off-gas composition depends on temperature and pressure in the furnace. Therefore, the experiments were done at a constant pressure and temperature in the furnace. Figure 11 shows the experimental results for a furnace temperature of 1000 °C and a pressure of about 1013 hPa.

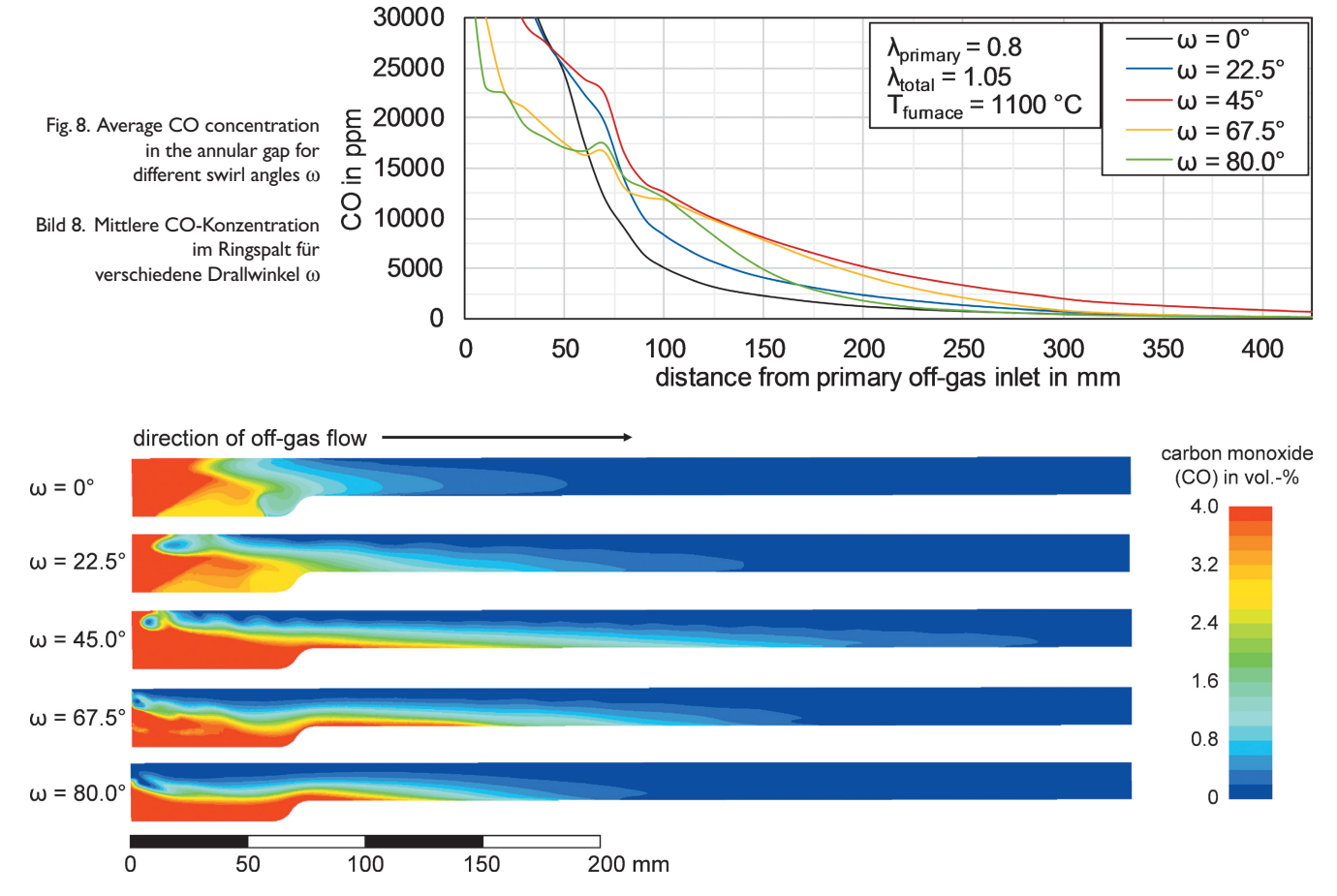


Fig. 9. Contour plots of the CO concentration in the annular gap for different swirl angles $\boldsymbol{\omega}$

Bild 9. CO-Konzentration über den Querschnitt des Ringspalts für verschiedene Drallwinkel ω

The primary air ratio was varied from $\lambda_{primary}=0.7$ to $\lambda_{primary}=0.9$, while the total air ratio after post-combustion was varied in a range from $\lambda_{total}=1.10$ to $\lambda_{total}=1.20$. Due to non-ideal mixing in the primary combustion chamber, the natural gas had not fully reacted to CO and H_2 and small amounts of CH_4 were detected.

The CO concentration of the off-gas after post-combustion was measured for a primary air ratio of $\lambda_{primary} = 0.7$ and different furnace temperatures $T_{furnace}$. The results are shown in Figure 12. The values were normalized on a basis of 3 vol.-% O_2 in the dry off-gas and shown in mg/m³ according to [14]. At a total air ratio of $\lambda_{total} = 1.10$, the CO concentration of the off-gas varies between

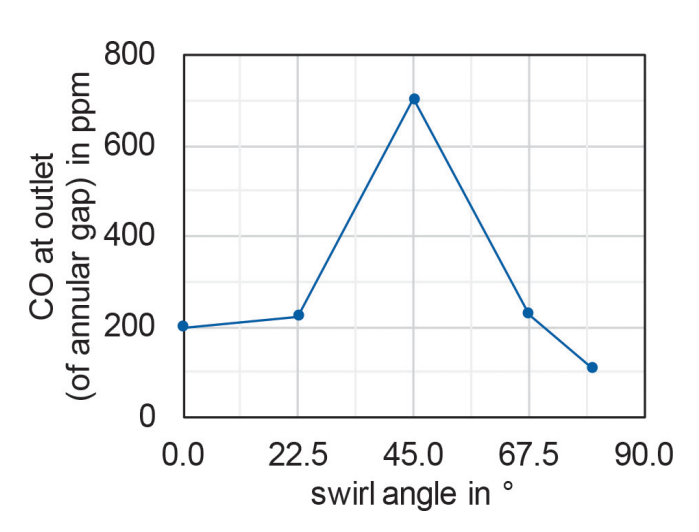


Fig. 10. Calculated CO concentration at the outlet of the annular gap

Bild 10. Berechnete CO-Konzentration am Ende des Ringspalts

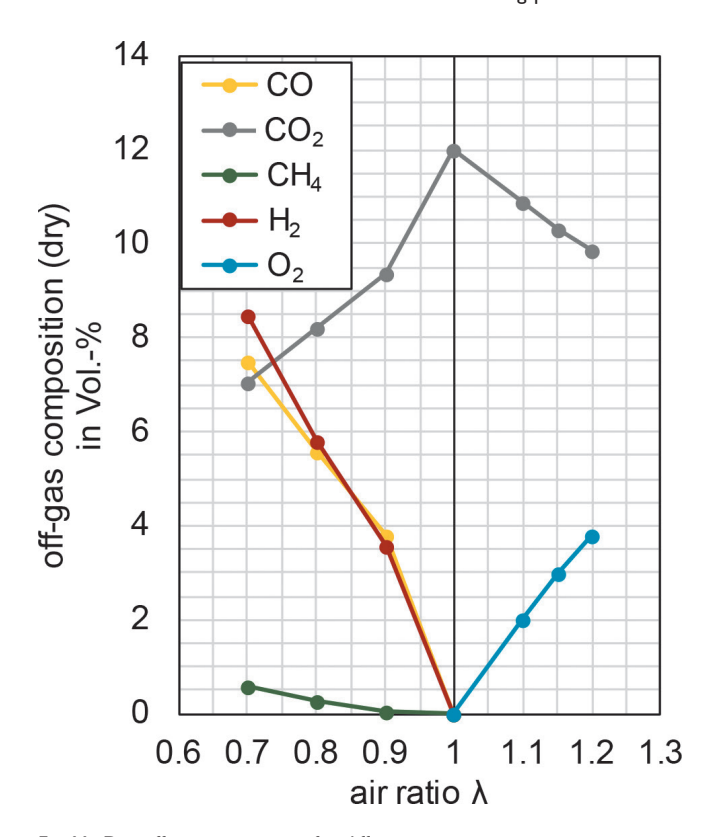


Fig. 11. Dry off-gas composition for different air ratios

Bild 11. Trockene Abgaszusammensetzung für verschiedene Luftzahlen

230 and 308 mg/m³. Higher total air ratios lead to values lower than 50 mg/m³.

In addition, the nitrous oxide emissions are determined via a NO and NO_2 measurement. The measured NO_x concentration for different air ratios and furnace temperatures is shown in Figure 13.

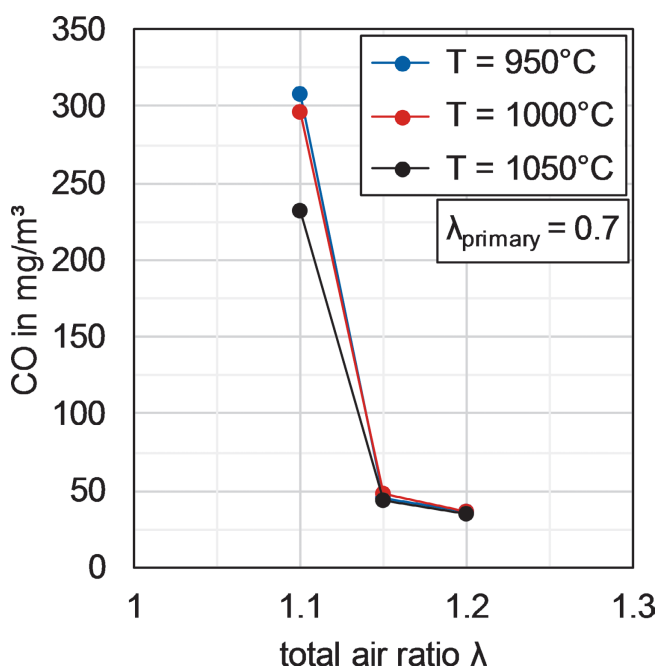


Fig. 12. Measured CO concentration after post-combustion for for different furnace temperatures $T_{\rm furnace}$

Bild 12. Gemessene CO-Konzentration nach Nachverbrennung für verschiedene Ofentemperaturen $\mathsf{T}_\mathsf{furnace}$

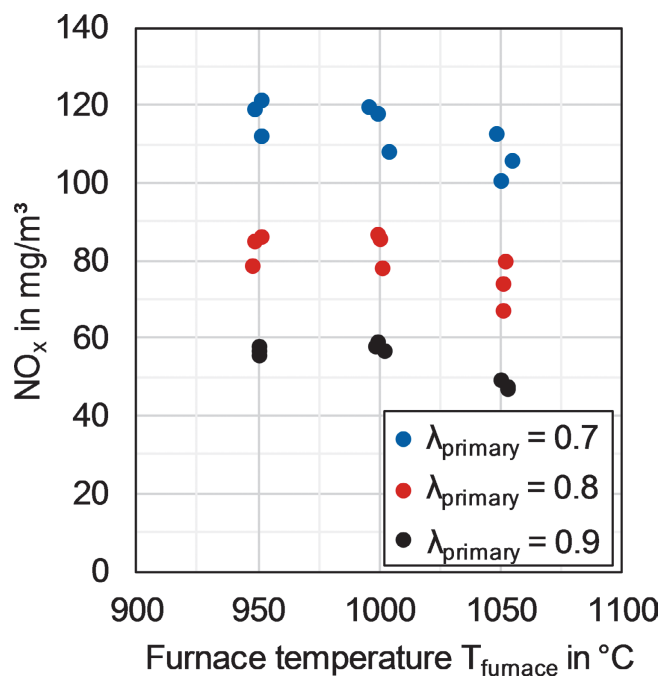


Fig. 13. Measured $NO_{\rm x}$ concentration after post-combustion for different primary air ratios $\lambda_{\rm primary}$

Bild 13. Gemessene ${
m NO}_x$ -Konzentration nach Nachverbrennung für verschiedene primäre Luftzahlen $\lambda_{\rm primary}$

There was a low dependence of the furnace temperature and the total air ratio on the NO_x -emissions. Furthermore, the primary air ratio $\lambda_{primary}$ has a large impact on the NO_x -emissions. For a primary air ratio of $\lambda_{primary} = 0.7$ the NO_x -emissions were in the range of 101 to 121 mg/m³. A higher primary air ratio means that less enthalpy is transformed into heat in the annular gap leading to lower maximum temperatures. This causes lower NO_x -emissions for $\lambda_{primary} = 0.8$ and $\lambda_{primary} = 0.9$ which were in the ranges of 67–87 mg/m³ and 47–57 mg/m³, respectively.

5 Discussion and summary

A common approach for the reheating of semi-finished metal products is direct heating with an oxidizing atmosphere by to the combustion of natural gas and air. In this study the development of a burner that combines a low oxidizing / reducing atmosphere due to fuel rich combustion, post-combustion in an open radiant tube (ORT) and a high recuperation of the off-gas for air preheating was presented.

A concept-burner was developed and first tested in numerical studies. The numerical model was capable to describe the flow field, the post-combustion and heat transfer. The computational domain included 1/16 of the annular gap formed between the ORT and the burner which started at the primary off-gas inlet and ended at the inlet of the recuperator. After a mandatory grid study, the swirl angle of the secondary air inlet was varied to determine the impact on the flow field and the post-combustion. Because of the high inlet velocities of the secondary air, the fluid flow in the annular gap was highly affected by the swirl angle. The swirl led to an outside drift of the air. This had an impact on the mixing performance of primary off-gas and secondary air and resulted in a low CO concentration at the outlet of the annular gap for a swirl angle of $\omega=0^\circ$ and $\omega=80^\circ$. Instead the maximum CO concentration was observed at a swirl angle of $\omega=45^\circ$.

In experimental tests, the concept-burner showed a solid performance especially concerning CO- and NO_x-emissions after the post-combustion. At a total air ratio of $\lambda_{total} > 1.1$, the CO-concentration in the off-gas was lower than 50 mg/m³ for all cases. Unlike carbon monoxide, the nitrous oxide emissions were strongly affected the primary air ratio $\lambda_{primary}$ and a lower primary air ratio resulted in increasing NO_x-emissions. Nevertheless, the total emission was lower than 121 mg/m³ for all cases.

In the next steps, the temperature and off-gas composition profile in the annular gap will be measured for the validation of the numerical model. After that, the numerical model will be used to design a ceramic prototype of the burner for high temperature processes. Further experimental investigations will be done to investigate the performance of the whole system, especially the combustion efficiency.

Acknowledgements

This project is supported by the Federal Ministry for Economic Affairs and Energy on the basis of a decision by the German Bundestag.

Danksagung

Das Projekt wird gefördert durch das Bundesministerium für Wirtschaft und Energie aufgrund eines Beschlusses des Deutschen Bundestages.

References

- Pfeifer, H.; Nacke, B.; Beneke, F.: Handbook of Thermoprocessing Technologies Volume 1: Fundamentals, Processes, Calculations. 2. ed., Vulkan-Verlag, Essen, 2010
- Abuluwefa, H. T.; Guthrie, R. I. L.; Ajersch, F.: The Effect of Oxygen Concentration on the Oxidation of Low-Carbon Steel in the Temperature Range 1000 to 1250 °C. Oxidation of Metals 46 (1996) 5/6, pp. 423-440
- Birks, N.; Meier, G. H.; Pettit, F. S.: Introduction to the High Temperature Oxidation of Metals. 2. ed., Cambridge University Press, Cambridge, UK, 2006
- 4. Atkinson, A.: Transport processes during the growth of oxide films at elevated temperature. Rev. Mod. Phys. 57 (1985) 2, pp. 437–470, DOI:10.1103/revmodphys.57.437
- Friedel, F.; Bolt, H.; Cornet, X.; Bourdon, G.; Vanden Eynde, X.; Zeimetz, E.; Ehlers, S.; Steinert, F.: Investigation of the formation, constitution and properties of scale formed during the finishing, rolling, cooling and coiling of thin hot strips. Technical Steel Research, Report EUR 21128 EN, Europ. Commission, Brussels, Belgium, 2004
- 6. Schmidt, R.; Winning, G.; Bender, W.; Hatzfeld, O.; Adler, W.: Weiterentwicklung und Betriebseinführung von Verfahren zur Umweltentlastung am Beispiel Schmiedeöfen durch Einsatz neuartiger Beheizungs-und Prozesstechnologien bei Hochtemperatur. Abschlussbericht über ein Forschungsvorhaben der Deutschen Bundesstiftung Umwelt, Nr. 14292, Kind & Co, Edelstahlwerk, in Zusammenarbeit mit BFI VDEh-Institut für angewandte Forschung GmbH, Wiehl, 2004
- Nemenyi, R.: Controlled Atmospheres for Heat Treatment. 1. ed., Pergamon Press, Oxford, UK, 1984
- Schwotzer, C.; Schnitzler, M.; Pfeifer, H.: Zunderarme Wiedererwärmung von Metall-Halbzeugen mit Rekuperatorbrennern. Gaswärme International 65 (2016) 3, pp. 67-72
- Schwotzer, C.; Schnitzler, M.; Pfeifer, H.; Ackermann, H.; Lucka, K.: Experimental investigation of a concept for scale free reheating of semi-finished metal products. Proc. 7th Europ. Combustion Meeting, 30.03-02.04.15, Budapest, Hungary, 2015, P2.53
- Schwotzer, C.; Balkenhol, T.; Schnitzler, M.; Pfeifer, H.; Ackermann, H.; Lucka, K.: Experimental investigation of a concept for scale free reheating of semi-finished metal products. Proc. 10th Europ. Conf. on Industrial Furnaces and Boilers, 07-10.04.15, Porto, Portugal, 2015
- Wuenning, J. G.; Milani, A.: Handbook of Burner Technology for Industrial Furnaces. 2. ed., Vulkan-Verlag, Essen, 2016
- Menter, F. R.: Two-Equation Eddy-Viscosity Turbulence Models for Engineering Applications. AIAA Journal 32 (1994) 8, pp. 1598-1605, DOI:10.2514/3.12149
- Magnussen, B. F.: The Eddy Dissipation Concept A Bridge between Science and Technology. Proc. ECCOMAS Thematic Conf. on Computational Combustion, 21-24.06.05, Lisbon, Portugal, 2005
- Bundesministerium für Umwelt Naturschutz und Reaktorsicherheit: Erste Allgemeine Verwaltungsvorschrift zum Bundes-Immissionsschutzgesetz (Technische Anleitung zur Reinhaltung der Luft), 2002

Bibliography

DOI:10.3139/105.110314 HTM J. Heat Treatm. Mat. 72 (2017) 2; page 73-80 © Carl Hanser Verlag GmbH & Co. KG ISSN 1867-2493